arXiv:2203.05958v4 [quant-ph] 24 Nov 2022

The Category of Linear Optical Quantum Computing

Paul McCloud
Department of Mathematics, University College London

November 28, 2022

Abstract

This note reviews the model of computation generated by photonic circuits, comprising edges that are traversed by photons in a single time-bin and vertices given by idealised lossless beam splitters and phase shifters. The circuit model is abstracted as a representation of the symmetric monoidal category of unitary matrices on the bosonic Fock space of multimode photons. A diagrammatic language, designed to aid with the understanding and development of photonic algorithms, is presented that encapsulates the category properties of this representation. As demonstrations of the formalism, the boson sampling scheme and the protocol of Knill, Laflamme and Milburn are developed on the single-rail photonic computer, and a parity-based model for the qudit is investigated.

Photonic circuits perform complex mathematical operations by exploiting the quantum mechanical properties of photons. The circuit is represented by a graph, with directed edges traversed by photons in a fixed unit of time (the 'time-bin'), and vertices given by idealised lossless beam splitters combined with phase shifters. Photons travel from one edge of the graph to the next over each time-bin, proceeding from the input edges through the internal edges to the output edges.

Each edge is associated with the state space of the photons that occupy it within a time-bin, and each vertex is associated with an operation that maps from the state space of its input edges to the state space of its output edges. Circuits constructed in this way are then combined according to the rules of symmetric monoidal categories. The circuit is thus characterised as an operation on a quantum system with input and output state on its external edges and internal state on its internal edges.

Author email: p.mccloud@ucl.ac.uk

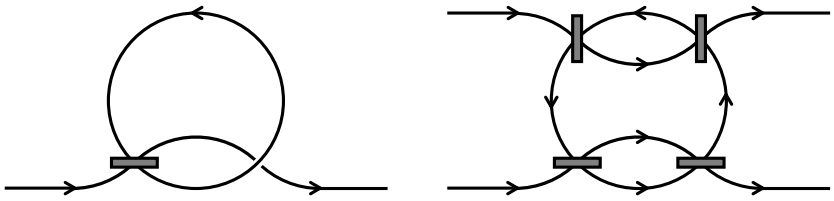


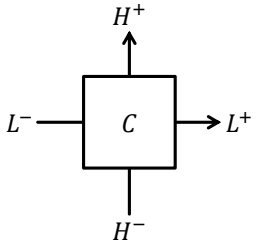
Figure 1: Examples of photonic circuits. The first example has single input and output edges, and a single internal edge that interferes with the input via a single beam splitter. The second example has two input and output edges, and six internal edges that interfere with the inputs and each other via four beam splitters. Complexity is increased by adding beam splitters, expanding the set of parameters available and enabling the construction of sophisticated graph topologies.

Beam splitters are configured to varying degrees of interference for the incident photons, generating transformations on the state space of the photons that become the functions of the corresponding model of computation. These functions are parametrised by the transmittance and reflectance of the beam splitters and the topology of the graph. Computation on the internal edges is seeded with photons prepared on the input edges and controlled according to measurements on the output edges. The objective of this essay is to identify the family of computations that can be performed on these circuits.

1 Circuit building

The circuit model is abstracted in a symmetric monoidal category that comprises systems and the operations that act between them. The rules of the category encapsulate the commonalities of these operations across a wide range of theoretical and physical models. Requiring no further assumptions at this stage, the category establishes a platform for the constructions in circuit building.

The systems considered in this essay are characterised as having external and internal subsystems, a decomposition that constrains the methods by which they are composed. During a single time-bin, the circuit implements an operation:

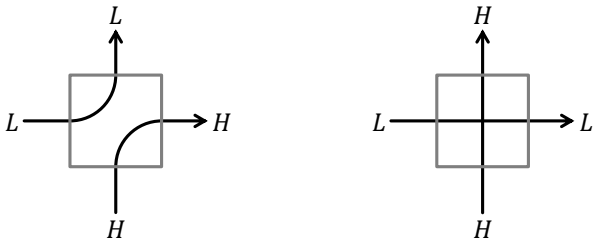


$$C : L^- \otimes H^- \to H^+ \otimes L^+ \tag{1}$$

where H^- is the input system and H^+ is the output system of the circuit.

Completing the definition, the internal system of the circuit is L^- before the operation and L^+ after the operation. Systems are represented in the diagram as legs attached to the sides of the box that represents the operation; by convention, the leg is omitted when it represents the empty system, the monoidal unit of the category. For notational convenience, unitor and associator operations are omitted in the following where they are unambiguous from the context.

As elementary examples, the identity and twist operations of the category generate the operations:



$$\iota \otimes \iota : L \otimes H \to L \otimes H \qquad \tau : L \otimes H \to H \otimes L \tag{2}$$

The first operation, the mirror, is given by the identity and the second operation, the window, is given by the twist. These operations exist for any pair of systems H and L and are combined to generate arbitrary system permutations.

Decomposing the system into its external and internal components, circuit building is limited to two types of composition – *spatial* and *temporal* – each corresponding to a specific physical arrangement. These compositions make a distinction between the external system, which can only be spatially connected to other circuits, and the internal system, which can only be temporally connected to other circuits.

Spatial composition is permitted for operations whose external systems are compatible, $H_1^+ = H_2^-$:

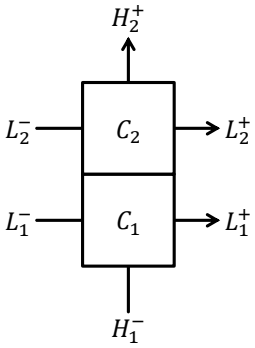
$$\begin{aligned} C_1 \oplus C_2 &= (\iota \otimes C_1) \circ (C_2 \otimes \iota) \\ &: (L_2^- \otimes L_1^-) \otimes H_1^- \to H_2^+ \otimes (L_2^+ \otimes L_1^+) \end{aligned} \tag{3}$$

This corresponds to the physical connection of two circuits at their shared external system. Temporal composition is permitted for operations whose internal systems are compatible, $L_1^+ = L_2^-$:

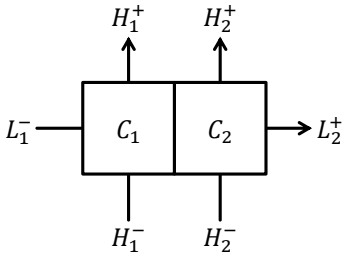
$$\begin{aligned} C_1 \ominus C_2 &= (C_1 \otimes \iota) \circ (\iota \otimes C_2) \\ &: L_1^- \otimes (H_1^- \otimes H_2^-) \to (H_1^+ \otimes H_2^+) \otimes L_2^+ \end{aligned} \tag{4}$$

This corresponds to the execution of the circuit over two consecutive time-bins. The categorical properties of these compositions are summarised in the table:

	Spatial	**Temporal**
Compatibility condition:	$H_1^+ = H_2^-$	$L_1^+ = L_2^-$
Input system:	H_1^-	$H_1^- \otimes H_2^-$
Output system:	H_2^+	$H_1^+ \otimes H_2^+$
Initial internal system:	$L_2^- \otimes L_1^-$	L_1^-
Final internal system:	$L_2^+ \otimes L_1^+$	L_2^+

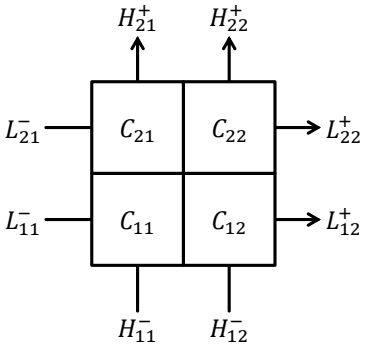


$$C_1 \oplus C_2 = (\iota \otimes C_1) \circ (C_2 \otimes \iota)$$



$$C_1 \ominus C_2 = (C_1 \otimes \iota) \circ (\iota \otimes C_2)$$

Figure 2: Circuits are constructed from elementary operations via composition. Spatial composition connects externally-compatible circuits at their common external system. Temporal composition executes internally-compatible circuits over consecutive time-bins.



$$(C_{11} \oplus C_{21}) \ominus (C_{12} \oplus C_{22}) = (C_{11} \ominus C_{12}) \oplus (C_{21} \ominus C_{22})$$

Figure 3: Spatial and temporal composition satisfy the interchange law, allowing their order of combination to be switched for compatible operations.

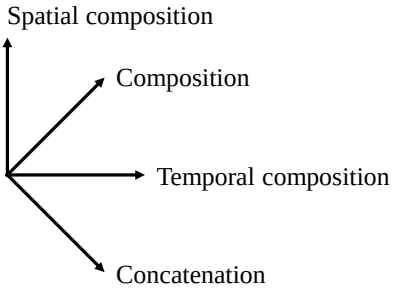
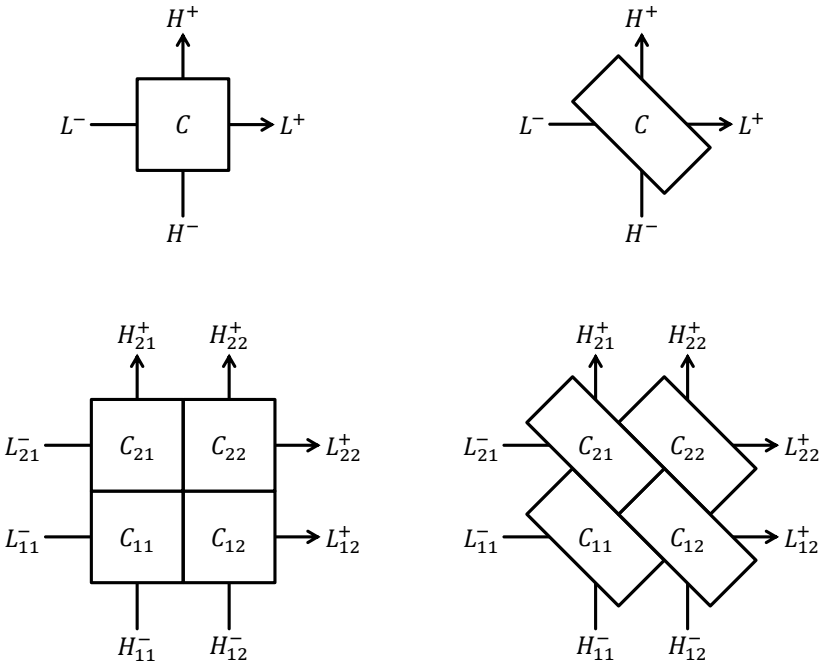


Figure 4: The binary operands of spatial composition $\oplus$ and temporal composition $\ominus$ are constructed from the elementary binary operands of composition $\circ$ and concatenation $\otimes$ in the monoidal category. These operands combine along rotated axes in the diagrammatic language, offering two equivalent perspectives for the combinations of operations.



$$(C_{11} \oplus C_{21}) \ominus (C_{12} \oplus C_{22}) = (C_{11} \ominus C_{12}) \oplus (C_{21} \ominus C_{22})$$
$$= (\iota \otimes C_{11} \otimes \iota) \circ (C_{21} \otimes C_{12}) \circ (\iota \otimes C_{22} \otimes \iota)$$

Figure 5: Two perspectives on the combinations of compatible operations. On the left, operations are combined using spatial and temporal composition. On the right, operations are combined using composition and concatenation. The equivalence between these perspectives derives the interchange law.

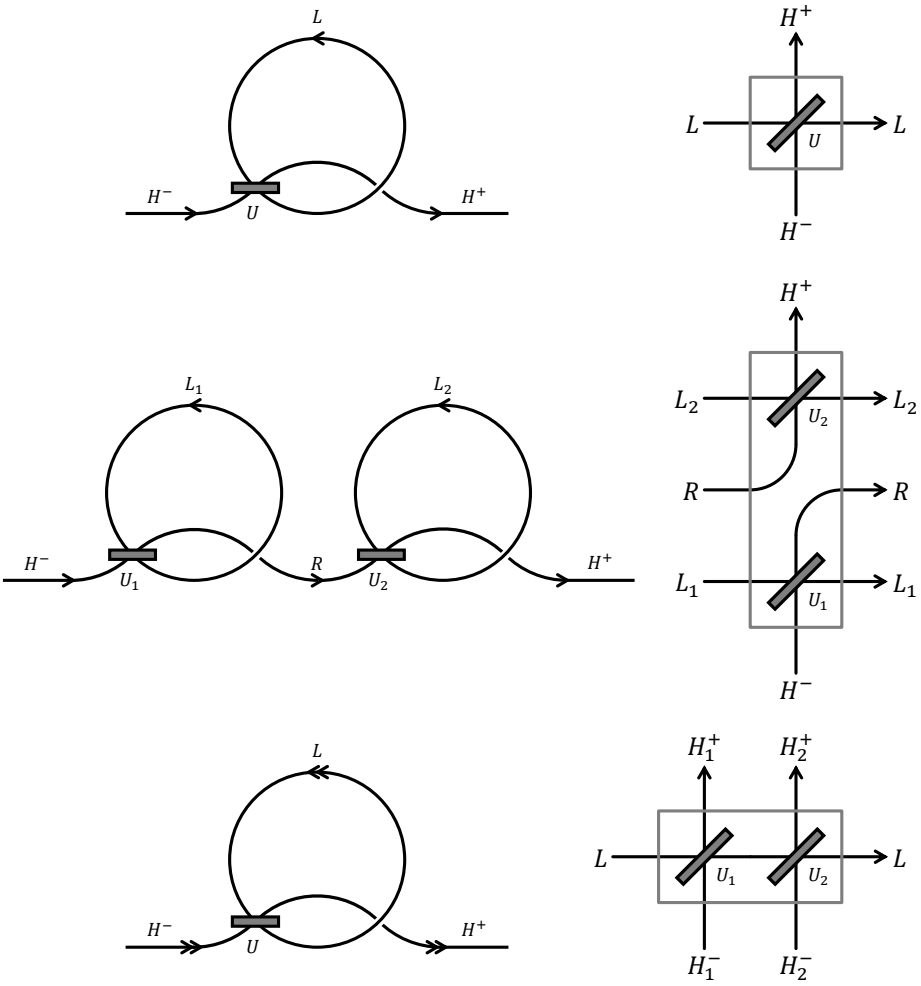


Figure 6: Photonic circuit building. In these examples, the single-loop circuit defined at the top is composed to generate two-loop circuits. Spatial composition connects two loops at their common external edge. Temporal composition creates a two-loop circuit by repeating the loop over two consecutive time-bins.

Composition simplifies when the internal system of the circuit is trivial, with spatial composition reducing to composition $C_1 \oplcirc C_2 = C_1 \circ C_2$ and temporal composition reducing to concatenation $C_1 \ominus C_2 = C_1 \otimes C_2$.

Spatial and temporal composition satisfy the interchange law:

$$\begin{aligned}(C_{11} \oplcirc C_{21}) \ominus (C_{12} \oplcirc C_{22}) &= (C_{11} \ominus C_{12}) \oplcirc (C_{21} \ominus C_{22}) \\ &= (\iota \otimes C_{11} \otimes \iota) \circ (C_{21} \otimes C_{12}) \circ (\iota \otimes C_{22} \otimes \iota)\end{aligned} \tag{5}$$

While these compatible operations are composed in different ways – spatial then temporal on the left, and temporal then spatial on the right – they arrive at the same combination. This freedom is used below to decompose the computer into operations representing preparation, computation and measurement.

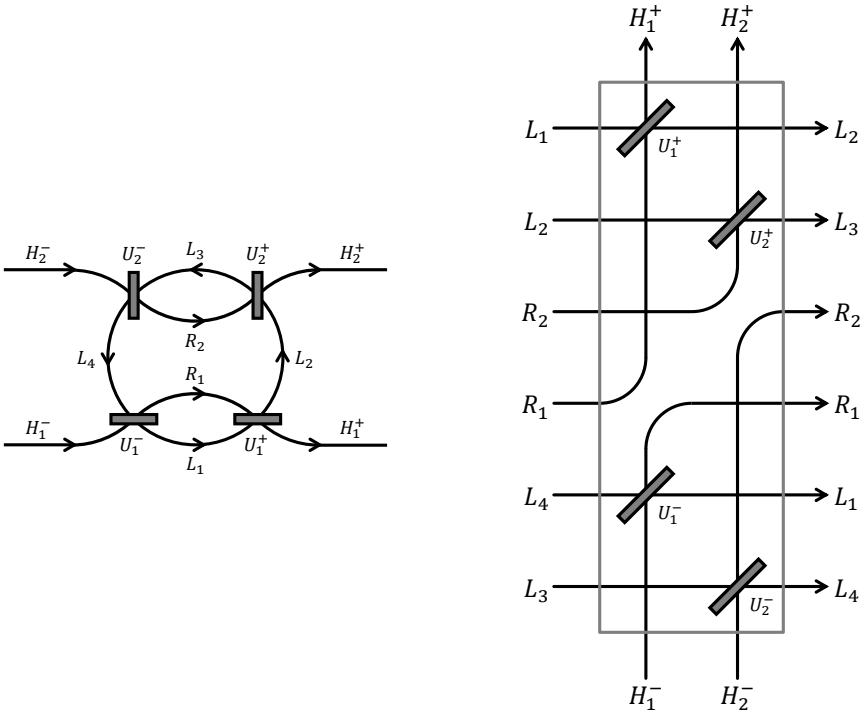
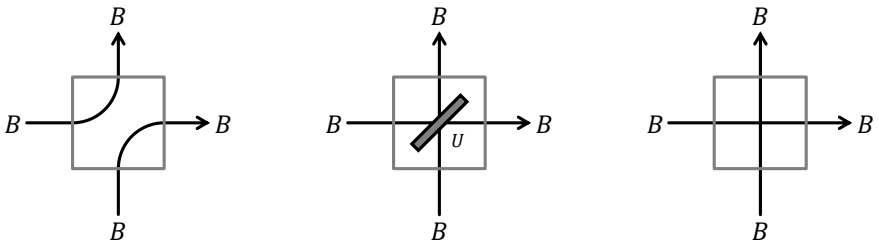


Figure 7: In this example of a photonic circuit, the operation on the external and internal edges over a single time-bin is represented by the diagram on the right, formally constructed from mirrors, windows and beam splitters.

Armed with these methods of composition, the circuit model is completed by introducing a toolkit of elementary operations. Photonic circuits introduce the *beam splitter*, which interpolates between the mirror and the window:

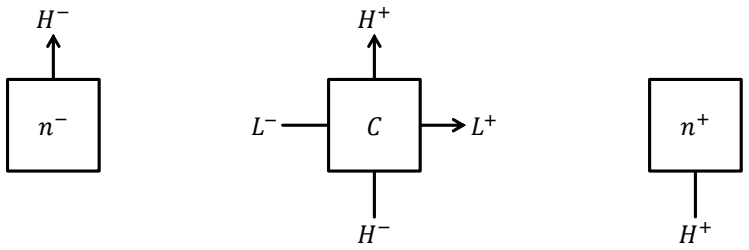


for the photonic system B. This operation is novel to the photonic circuit model, extending the elementary operations of the symmetric monoidal category by enabling interference between systems. Quantum advantage in the model of computation emerges from the extension of the discrete permutation group generated by mirrors and windows to the continuous unitary group generated by beam splitters. Classical logic gates, presented as permutations on classical bits, are reinterpreted as unitary transformations on quantum bits in superpositions. This argument is developed in the following sections.

2 Computation

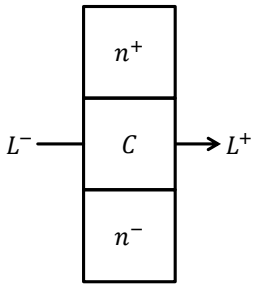
The partition of the system into its external and internal subsystems is reflected in the model of computing. The programmer interacts with the external system, preparing the input state and measuring the output state. Sandwiched between these operations, computation is performed on the internal system.

In its canonical form, execution of the circuit is comprised of three operations representing preparation, computation and measurement:



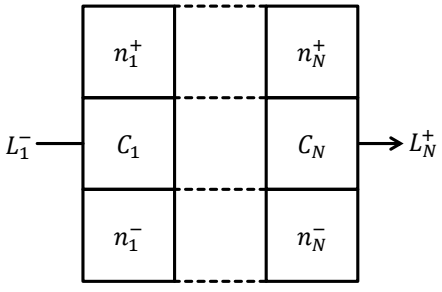
$$\langle n^-| : \to H^- \qquad C : L^- \otimes H^- \to H^+ \otimes L^+ \qquad |n^+\rangle : H^+ \to \quad (6)$$

These operations are spatially composed to generate the operation of the circuit on the internal state over a single time-bin:



$$\langle n^-| \oplus C \oplus |n^+\rangle = (\iota \otimes \langle n^-|) \circ C \circ (|n^+\rangle \otimes \iota) \quad (7)$$

Repeated execution over multiple time-bins then generates the temporally composed operation on the internal state:



$$(\langle n_1^-| \oplus C_1 \oplus |n_1^+\rangle) \circ \cdots \circ (\langle n_N^-| \oplus C_N \oplus |n_N^+\rangle) \quad (8)$$
$$= (\langle n_1^-| \otimes \cdots \otimes \langle n_N^-|) \oplus (C_1 \ominus \cdots \ominus C_N) \oplus (|n_1^+\rangle \otimes \cdots \otimes |n_N^+\rangle)$$

where the interchange law is used to express the total operation of the circuit over multiple time-bins in canonical form, identifying the total computation as the temporal composition of the computations in each time-bin.

Abstracted in this way, the model has the three elements essential for a computer: an internal register where computation is performed; a means to write data into the register; and a means to read data from the register. For the quantum computer, the physical components that implement these operations exploit the properties of quantum mechanics, summarised in two postulates that describe the evolution of the quantum system and its interaction with the external system.

To understand how these operations manifest in the quantum computer requires specialisation to the category of quantum mechanics, wherein systems are represented as separable Hilbert spaces and operations are bounded linear maps between the spaces they connect, by convention acting from left to right in the following. The monoidal unit is the trivial Hilbert space $\mathbb{C}$ and the monoidal product is the Hilbert space tensor product $\otimes$. In this category, the state $\langle n| \in H$ is associated with two mutually-adjoint bounded linear maps:

$$\begin{aligned} \langle n| &: \mathbb{C} \to H : \lambda \mapsto \lambda \langle n| \\ |n\rangle &: H \to \mathbb{C} : \langle m| \mapsto \langle m|n\rangle \end{aligned} \tag{9}$$

utilised for preparation and measurement. Computation is then a unitary map:

$$C : L^- \otimes H^- \to H^+ \otimes L^+ \tag{10}$$

that models the physical evolution of the system over a single time-bin.

Formulated for the application to computing, the first assumption of quantum mechanics identifies the transformation of the internal state generated by the quantum circuit.

Assumption 1 (Quantum Mechanics)**.** *If the input system is prepared in the state $\langle n^-| \in H^-$ and the output system is measured in the state $\langle n^+| \in H^+$, then execution of the circuit effects the transformation of the internal state:*

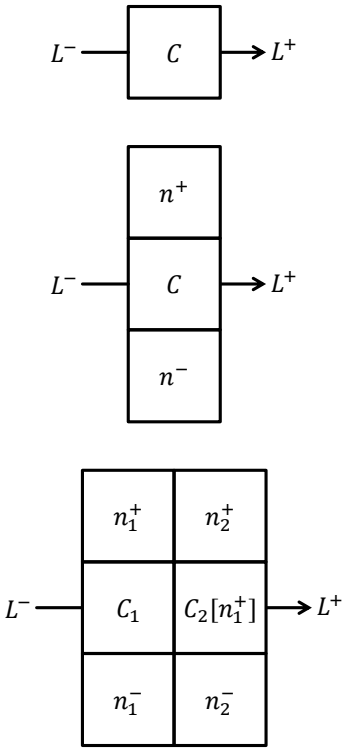
$$\langle n^-|C|n^+\rangle := \langle n^-| \oplus C \oplus |n^+\rangle : L^- \to L^+ \tag{11}$$

This transformation combines the evolution of the internal system and its interaction with the external system, and both these effects have algorithmic content for the computer.

The apparatuses of the external system are associated with orthonormal bases that diagonalise their target families of commuting observables, with the prepared state drawn from the preparation basis and the measured state drawn from the measurement basis. Expressing the essentially indeterminate nature of this procedure, the fundamental asymmetry between preparation and measurement is encapsulated in the second assumption of quantum mechanics.

Assumption 2 (Quantum Mechanics)**.** *If the internal system is initially in the state $\langle m| \in L^-$ and the input system is prepared in the basis state $\langle n^-| \in H^-$, then the output system is measured in the basis state $\langle n^+| \in H^+$ with probability:*

$$\left\| \langle m|\langle n^-|C|n^+\rangle \right\|^2 / \left\| \langle m| \right\|^2 \tag{12}$$



Quantum processes are described by unitary maps, which provide the basic algorithmic components of the quantum circuit.

Measurement-based computing expands the range of operations available on the circuit by exploiting projective measurement:

$$\langle n^-|C|n^+\rangle$$

This is successful only when the output is measured in the required state.

Combined with projective measurement, the feed-forward protocol further expands the range of available operations:

$$\langle n_1^-|C_1|n_1^+\rangle\,\langle n_2^-|C_2[n_1^+]|n_2^+\rangle$$

This is used to optimise the probability of successful implementation.

Figure 8: The physical process implements a unitary map in the quantum computer. Projective measurement and the feed-forward protocol augment this with the transformative effect of measurement to build algorithmic complexity.

Data is extracted from the computation by estimating these probabilities via repeated execution of the circuit.

The computer thus comprises a circuit engineered to implement the desired operation, coupled to apparatuses that prepare the input state and measure the output state in their associated orthonormal bases. Central to this calculation, the unitary map that describes the physical evolution of the total system decomposes into blocks that individually act on the internal state:

$$C = \sum_{\langle n^-|}\sum_{\langle n^+|} \langle n^+| \otimes \langle n^-|C|n^+\rangle \otimes |n^-\rangle \tag{13}$$

where the sums are over the preparation and measurement bases. Using the effect of *projective measurement*, the transformation of the internal state executed by the circuit is non-deterministic, extracting the block $\langle n^-|C|n^+\rangle$ from the computation C with row $\langle n^-|$ selected by the programmer but with column $\langle n^+|$ selected at random.

The algorithmic scope of the computer depends on the unitary operations that can be implemented on the physical system and the fidelity of the preparation and measurement apparatuses. The *feed-forward protocol* increases this scope by dynamically updating the circuit in response to measurements in pre-

ceding time-bins. Over two time-bins, the protocol generates an operation:

$$\begin{aligned}\langle n_1^-|C_1|n_1^+\rangle \langle n_2^-|C_2[n_1^+]|n_2^+\rangle \\ = (\langle n_1^-| \otimes \langle n_2^-|)(C_1 \ominus C_2)(|n_1^+\rangle \otimes |n_2^+\rangle)\end{aligned} \tag{14}$$

The interchange law derives the total computation as a temporal composition, using orthonormality of the measurement basis to extend the definition:

$$C_1 \ominus C_2 = (C_1 \otimes \iota) \sum_{\langle n_1^+|} (|n_1^+\rangle \langle n_1^+| \otimes C_2[n_1^+]) \tag{15}$$

While the practical challenges of dynamic updating in physical circuits should not be underestimated, this extended protocol for temporal composition greatly expands the algorithmic range.

The lack of determinism is a problem with an approach that utilises projective measurement. For a computer engineered to a specific task, the desired operation may not be implemented in all possible outcomes, with success or failure indicated by the measurement of the output state. Fortunately quantum mechanics presents a practical solution to this conundrum. Non-deterministic protocols can be used to prepare clusters of entangled states in advance of computation. Measurement-based computing then proceeds via targeted measurement of the cluster state resource, using the feed-forward protocol to generate the desired operation on the internal state.

3 Photonic operations

With the platform for circuit building established as the symmetric monoidal category of quantum systems, this section develops the family of operations generated by linear optical components acting on photons. Conveniently, these operations are described by a monoidal functor that represents unitary matrices on multimode bosonic Fock spaces.

The state space of indistinguishable photons in a single mode is the bosonic Fock space B, with vacuum state $\langle 0|$ and orthonormal computation basis given by states of the form:

$$\langle n| = \frac{1}{\sqrt{n!}} \langle 0|a^n \tag{16}$$

where the operation $a : B \to B$ is the photon creation operator on the state space. The N-mode state space $B[N]$ is the Nth tensor power of B, and the creation and annihilation operators a_M and a_M^* for the M-mode are:

$$\begin{aligned}\langle n_1 \cdots n_N|a_M &= \sqrt{n_M + 1}\ \langle n_1 \cdots (n_M + 1) \cdots n_N| \\ \langle n_1 \cdots n_N|a_M^* &= \sqrt{n_M}\ \langle n_1 \cdots (n_M - 1) \cdots n_N|\end{aligned} \tag{17}$$

The number operator $\hat{n}_M$ for the M-mode is then:

$$\hat{n}_M = a_M a_M^* - 1 \tag{18}$$

and the computation basis of the N-mode state space comprises the eigenstates for its family of number operators.

In the linear optical model, a computation in the photonic circuit is determined by its commutation relations with the creation operators on the state spaces of its edges. The operation:

$$B[U] : H^- \to H^+ \tag{19}$$

with state spaces $H^- = H^+ = B[N]$ is generated by a unitary N-matrix U via the commutation relations:

$$a_M B[U] = B[U] \sum_{L=1}^{N} U_{ML} a_L \tag{20}$$

These relations are sufficient to determine the operation on the basis states up to an overall normalisation:

$$\begin{aligned} \langle n_1 \cdots n_N | B[U] &= \left(\frac{1}{\sqrt{n_1! \cdots n_N!}} \langle 0 \cdots 0 | \prod_{M=1}^{N} a_M^{n_M}\right) B[U] \\ &= \frac{1}{\sqrt{n_1! \cdots n_N!}} \langle 0 \cdots 0 | \prod_{M=1}^{N} \left(\sum_{L=1}^{N} U_{ML} a_L\right)^{n_M} \end{aligned} \tag{21}$$

where the definition is completed with the normalisation:

$$\langle 0 \cdots 0 | B[U] = \langle 0 \cdots 0 | \tag{22}$$

on the vacuum state. Expanding the brackets and applying the creation operators to the vacuum state, this generates an operation that preserves the total photon number:

$$\langle n_1^- \cdots n_N^- | B[U] = \sum_{\substack{n_1^+ + \cdots + n_N^+ = \\ n_1^- + \cdots + n_N^-}} \langle n_1^- \cdots n_N^- | B[U] | n_1^+ \cdots n_N^+ \rangle \langle n_1^+ \cdots n_N^+ | \tag{23}$$

where the matrix elements of $B[U]$ on the eigenspace of total photon number n are linear combinations of products of n elements from U.

The map B as defined here is a monoidal functor. The source category of the functor comprises the strictly positive integers with unitary matrices in the corresponding dimensions. The target category of the functor comprises the multimode bosonic Fock spaces with the unitary maps they support. Monoidal functoriality for objects is the property:

$$B[N_1 + N_2] = B[N_1] \otimes B[N_2] \tag{24}$$

while monoidal functoriality for morphisms is the properties:

$$\begin{aligned} B[U_1 \oplus U_2] &= B[U_1] \otimes B[U_2] \\ B[U_1 U_2] &= B[U_1] B[U_2] \end{aligned} \tag{25}$$

for compatible unitary matrices. Photonic circuits thus create a representation of the category of finite-dimensional unitary matrices as unitary operations on the multimode bosonic Fock spaces of photons.

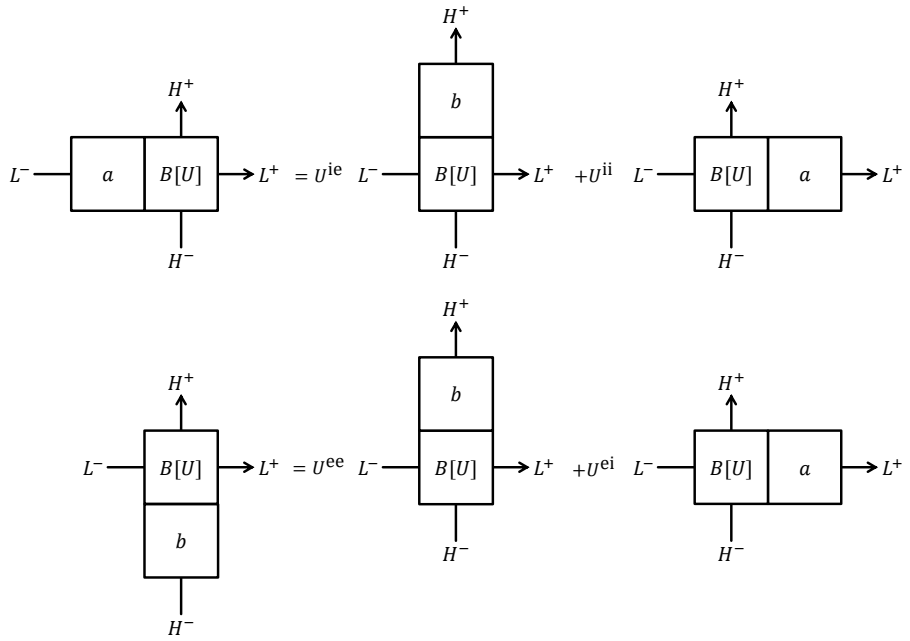


Figure 9: The commutation relations between a circuit $B[U]$ and the photon creation operators a on its internal edges and b on its external edges are generated from a unitary matrix U.

For the operation:

$$B[U] : L^- \otimes H^- \to H^+ \otimes L^+ \tag{26}$$

whose state spaces decompose into internal state spaces $L^- = L^+ = B[M]$ and external state spaces $H^- = H^+ = B[N]$, the unitary matrix U that generates the operation decomposes into blocks:

$$U = \begin{bmatrix} U^{\mathrm{ie}} & U^{\mathrm{ii}} \\ U^{\mathrm{ee}} & U^{\mathrm{ei}} \end{bmatrix} \tag{27}$$

where the superscript e indicates external edges and the superscript i indicates internal edges. The functorial nature of the map from the matrix U to the operation $B[U]$ that it generates allows the calculus of circuit building to be expressed by constructions within the category of finite-dimensional unitary matrices. This simplifies the analysis of circuits.

Consider the pair of operations:

$$\begin{aligned} B[U_1] &: L_1^- \otimes H_1^- \to H_1^+ \otimes L_1^+ \\ B[U_2] &: L_2^- \otimes H_2^- \to H_2^+ \otimes L_2^+ \end{aligned} \tag{28}$$

Compositions of these operations are efficiently described by the unitary matrices in their commutation relations. The operations are spatially compatible when $N_1 = N_2$, in which case the unitary matrix that generates the spatial

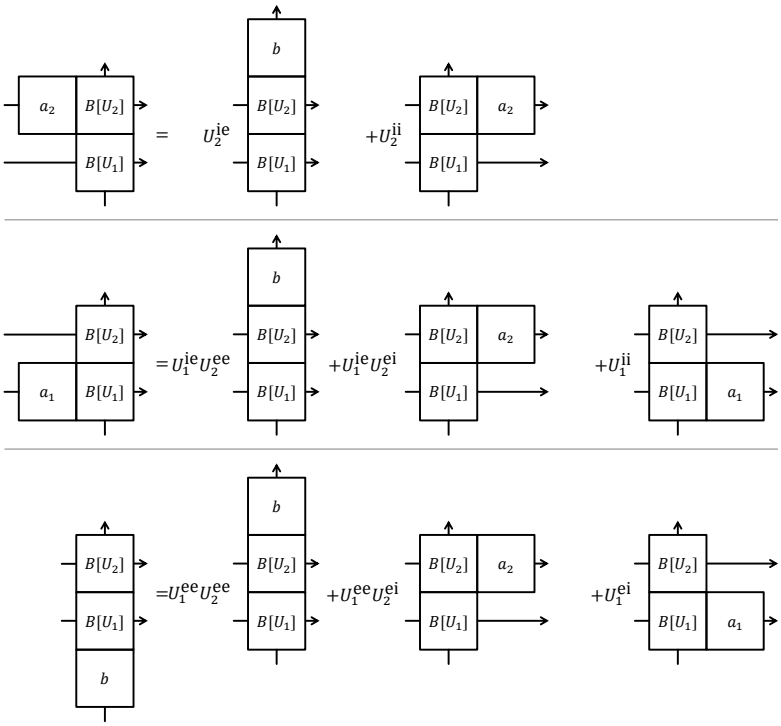


Figure 10: The unitary matrix that generates spatial composition is identified by commuting the photon creation operators through its two circuits.

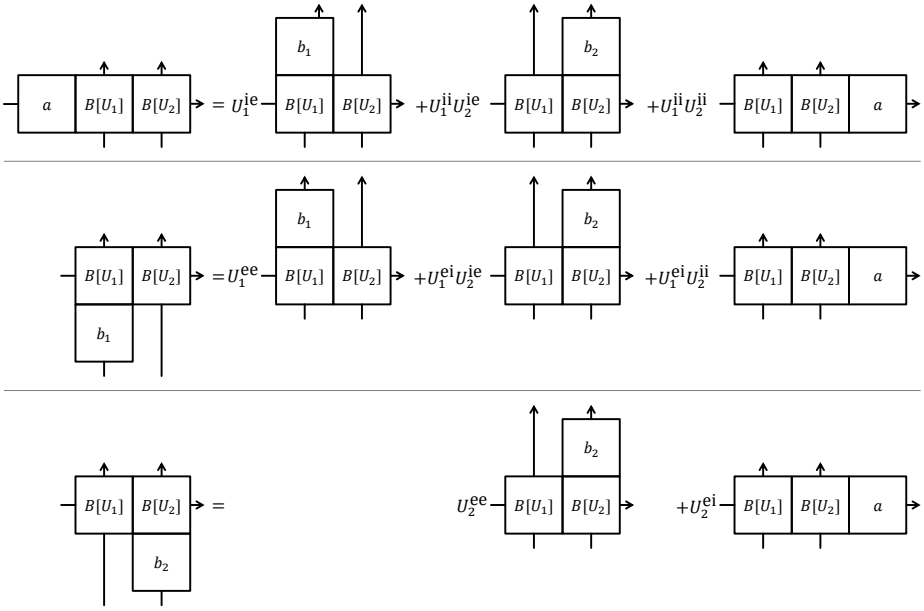


Figure 11: The unitary matrix that generates temporal composition is identified by commuting the photon creation operators through its two circuits.

composition is:

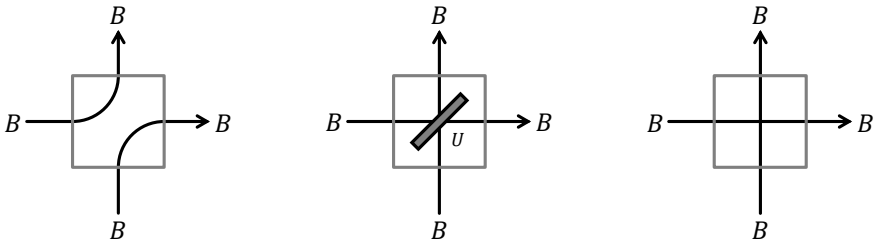
$$(1 \oplus U_1)(U_2 \oplus 1) = \begin{bmatrix} 1 & 0 & 0 \\ 0 & U_1^{\mathrm{ie}} & U_1^{\mathrm{ii}} \\ 0 & U_1^{\mathrm{ee}} & U_1^{\mathrm{ei}} \end{bmatrix} \begin{bmatrix} U_2^{\mathrm{ie}} & U_2^{\mathrm{ii}} & 0 \\ U_2^{\mathrm{ee}} & U_2^{\mathrm{ei}} & 0 \\ 0 & 0 & 1 \end{bmatrix} \tag{29}$$
$$= \begin{bmatrix} U_2^{\mathrm{ie}} & U_2^{\mathrm{ii}} & 0 \\ U_1^{\mathrm{ie}} U_2^{\mathrm{ee}} & U_1^{\mathrm{ie}} U_2^{\mathrm{ei}} & U_1^{\mathrm{ii}} \\ U_1^{\mathrm{ee}} U_2^{\mathrm{ee}} & U_1^{\mathrm{ee}} U_2^{\mathrm{ei}} & U_1^{\mathrm{ei}} \end{bmatrix}$$

The operations are temporally compatible when $M_1 = M_2$, in which case the unitary matrix that generates the temporal composition is:

$$(U_1 \oplus 1)(1 \oplus U_2) = \begin{bmatrix} U_1^{\mathrm{ie}} & U_1^{\mathrm{ii}} & 0 \\ U_1^{\mathrm{ee}} & U_1^{\mathrm{ei}} & 0 \\ 0 & 0 & 1 \end{bmatrix} \begin{bmatrix} 1 & 0 & 0 \\ 0 & U_2^{\mathrm{ie}} & U_2^{\mathrm{ii}} \\ 0 & U_2^{\mathrm{ee}} & U_2^{\mathrm{ei}} \end{bmatrix} \tag{30}$$
$$= \begin{bmatrix} U_1^{\mathrm{ie}} & U_1^{\mathrm{ii}} U_2^{\mathrm{ie}} & U_1^{\mathrm{ii}} U_2^{\mathrm{ii}} \\ U_1^{\mathrm{ee}} & U_1^{\mathrm{ei}} U_2^{\mathrm{ie}} & U_1^{\mathrm{ei}} U_2^{\mathrm{ii}} \\ 0 & U_2^{\mathrm{ee}} & U_2^{\mathrm{ei}} \end{bmatrix}$$

These expressions describe the mathematics of photonic circuit building in terms of the generating unitary matrices.

The basic operation in photonic circuit building is the beam splitter:



$$I = \begin{bmatrix} 1 & 0 \\ 0 & 1 \end{bmatrix} \qquad U = e^{i\gamma} \begin{bmatrix} e^{-i\rho} \sin[\theta] & e^{-i\tau} \cos[\theta] \\ e^{i\tau} \cos[\theta] & -e^{i\rho} \sin[\theta] \end{bmatrix} \qquad X = \begin{bmatrix} 0 & 1 \\ 1 & 0 \end{bmatrix} \tag{31}$$

The beam splitter has transmittance $\cos[\theta]^2$ and reflectance $\sin[\theta]^2$. Combined with phase shifters, the beam splitter introduces a global phase γ together with phase difference τ between the transmitted photons and phase difference ρ between the reflected photons. This creates any generating unitary matrix in two dimensions.

Elementary examples of configurations for the beam splitter include the mirror, with $\theta = \gamma = \rho = \pi/2$, and the window, with $\theta = \gamma = \tau = 0$. More generally, the operation is used to interfere the input photons and generate mixed states on the output edges. Beam splitters are then combined via spatial and temporal composition to create any generating unitary matrix in N dimensions.

Circuits constructed from this optical component include the single-rail photonic computer, a simple architecture which nonetheless implements a wide range of photonic operations.

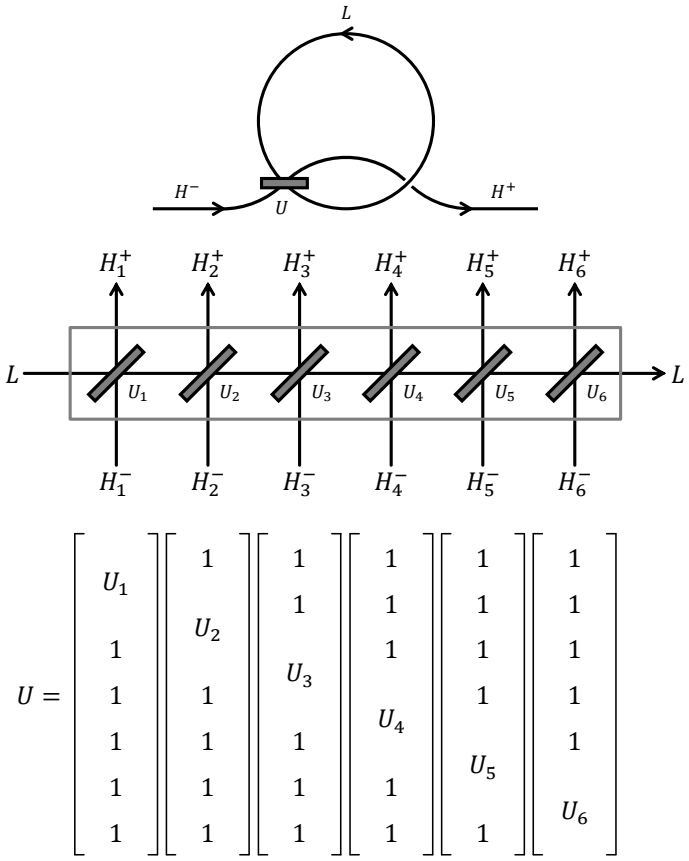


Figure 12: The single-loop photonic computer. The physical circuit comprises a single loop executed over N_H consecutive time-bins ($N_H = 6$ in this example). The generating unitary matrix of the operation is the product of N_H block-diagonal unitary matrices, represented here as the column vectors of their diagonal blocks.

The single-loop photonic computer. The simplest non-trivial photonic circuit is the single-loop circuit, with one input and output edge interfering with an internal edge via a configurable beam splitter.

The beam splitter is configured to the reflectance and phase shifts of a unitary 2-matrix U. When the input is prepared in the basis state $\langle n^-| \in H^-$ and the output is measured in the basis state $\langle n^+| \in H^+$, conservation of photon number implies that the action on the internal state is:

$$\langle m^-|\langle n^-|B[U]|n^+\rangle = \langle m^- n^-|B[U]|n^+ m^+\rangle \langle m^+| \tag{32}$$

where:

$$m^+ = m^- + n^- - n^+ \tag{33}$$

For such a simple circuit, this operation is surprisingly complex. The computer does not mix internal basis states but does transform the coefficients, with

amplitudes determined from the commutation relation as:

$$\begin{aligned}
&\langle m^- n^- | B[U] | n^+ m^+ \rangle = \\
&\sqrt{\frac{n^+! m^+!}{m^-! n^-!}} e^{i((m^- + n^-)\gamma - (m^- - n^+)\tau + (n^- - n^+)\rho)} \times \\
&(-)^{\min[n^-, m^+]} \cos[\theta]^{|m^- - n^+|} \sin[\theta]^{|n^- - n^+|} \times \\
&\sum_{\eta=0}^{\kappa} \binom{m^-}{\min[m^-, n^+] - \eta} \binom{n^-}{\min[n^-, n^+] - (\kappa - \eta)} (-)^{\eta} \cos[\theta]^{2\eta} \sin[\theta]^{2(\kappa - \eta)}
\end{aligned} \tag{34}$$

where:

$$\kappa = \min[m^-, n^+] + \min[n^-, n^+] - n^+ \tag{35}$$

These amplitudes demonstrate the trigonometric nature of interference between the photons incident on the beam splitter.

With careful alignment of the angles in successive time-bins, interference and projective measurement are exploited to create useful operations on the single-loop circuit. Since this depends on the output photon count, the target operation is implemented non-deterministically with success rate given by the squared modulus of the amplitude.

As an example, implementation of the non-linear sign gate on the single-loop photonic computer uses the following diagonal cases:

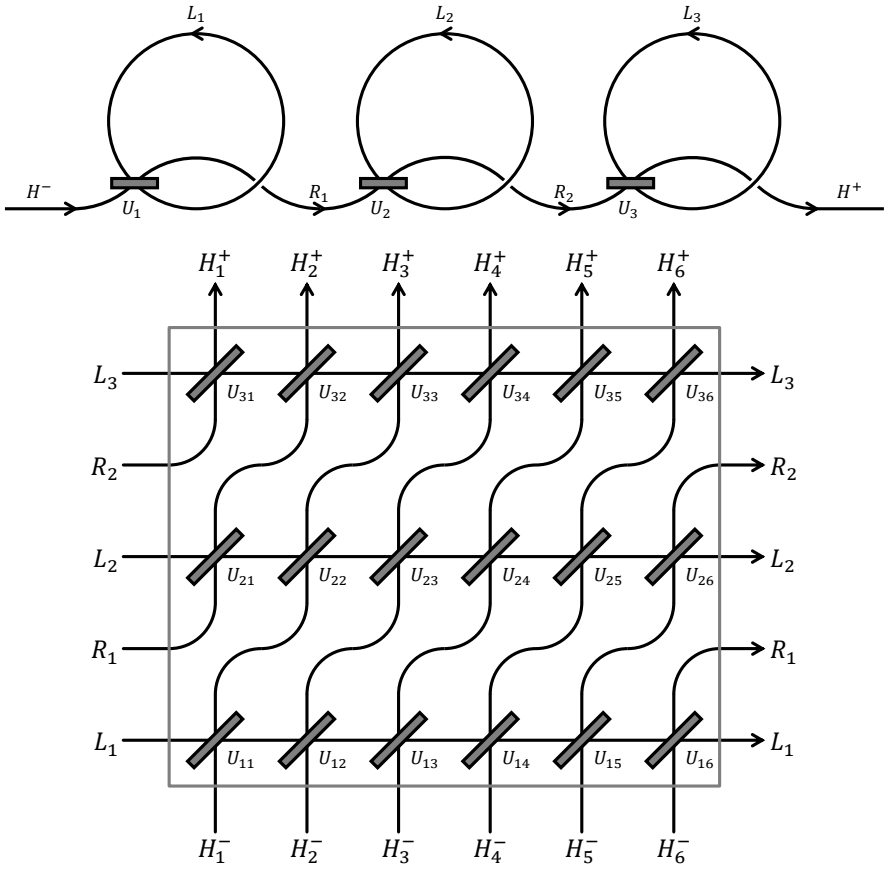
$$\begin{aligned}
\langle m | \langle 0 | B[U] | 0 \rangle &= e^{im(\gamma - \tau)} \cos[\theta]^m \langle m | \\
\langle m | \langle 1 | B[U] | 1 \rangle &= -e^{i((m+1)\gamma - (m-1)\tau)} \cos[\theta]^{m-1} (m - (1+m)\cos[\theta]^2) \langle m |
\end{aligned} \tag{36}$$

to change the sign of the internal basis state conditional on its photon count. This operation is integral to the Knill, Laflamme and Milburn implementation of the controlled-Z gate, which enables universal quantum computing on the single-rail circuit. Details of this implementation are presented later in the essay.

The single-rail photonic computer. The single-rail circuit is constructed by linking single-loop circuits at their external edges. Executing the circuit over successive time-bins generates a computer that is programmable through the configurations of the beam splitters at each stage.

The single-rail photonic computer with N_L loops has a total of $2N_L+1$ edges: one edge each as input and output; N_L edges forming the loops that hold the internal state for computation; and a rail comprising $N_L - 1$ linking edges that enable writing onto and reading from the loops. Each loop connects to the rail via a beam splitter. Executed over N_H consecutive time-bins, the computer thus has $N_L N_H$ programmable beam splitters creating a total operation generated by a unitary $(2N_L - 1 + N_H)$-matrix. Since the operation in each beam splitter is associated with a unitary 2-matrix, the total operation is generated by the product of N_H block-diagonal unitary $(2N_L - 1 + N_H)$-matrices, with non-trivial blocks given by the generating matrices of the beam splitters.

When the beam splitters are configured to be either mirrors or windows, photons entered on the input edges have a deterministic path through the circuit diagram. The map from input to output is then a permutation, mapping each input edge either to a unique output edge or to an internal edge. Any other



$$U = \begin{bmatrix} U_{31} \\ U_{21} \\ U_{11} \\ 1 \\ 1 \\ 1 \\ 1 \\ 1 \end{bmatrix} \begin{bmatrix} 1 \\ U_{32} \\ U_{22} \\ U_{12} \\ 1 \\ 1 \\ 1 \\ 1 \end{bmatrix} \begin{bmatrix} 1 \\ 1 \\ U_{33} \\ U_{23} \\ U_{13} \\ 1 \\ 1 \\ 1 \end{bmatrix} \begin{bmatrix} 1 \\ 1 \\ 1 \\ U_{34} \\ U_{24} \\ U_{14} \\ 1 \\ 1 \end{bmatrix} \begin{bmatrix} 1 \\ 1 \\ 1 \\ 1 \\ U_{35} \\ U_{25} \\ U_{15} \\ 1 \end{bmatrix} \begin{bmatrix} 1 \\ 1 \\ 1 \\ 1 \\ 1 \\ U_{36} \\ U_{26} \\ U_{16} \end{bmatrix}$$

Figure 13: The single-rail photonic computer. The physical circuit comprises a sequence of N_L loops ($N_L = 3$ in this example) executed over N_H consecutive time-bins ($N_H = 6$ in this example). The generating unitary matrix of the operation is the product of N_H block-diagonal unitary matrices, represented here as the column vectors of their diagonal blocks.

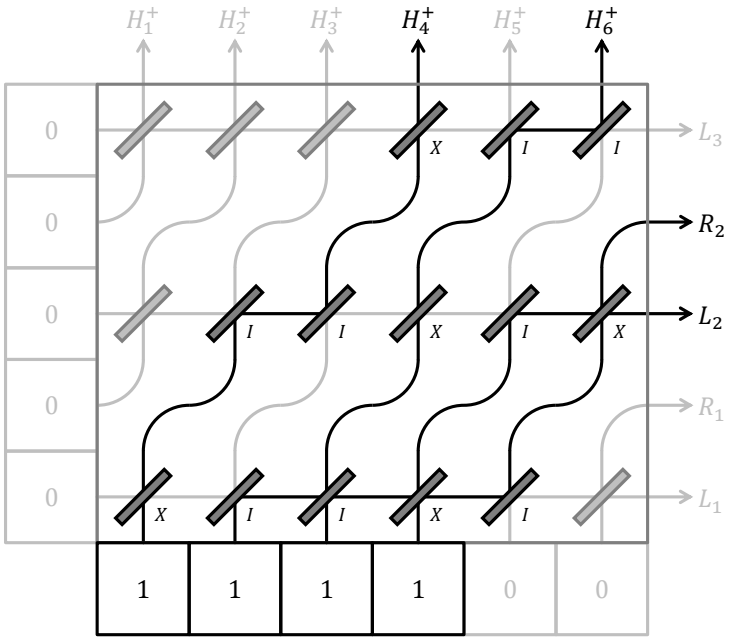


Figure 14: Tracking the input photons through a deterministic circuit with beam splitters configured either as mirrors or as windows, the resulting operation permutes the output photons. More generally, beam splitters create mixed states of photons on the output and internal edges in permutations determined by the topology of the graph. Complexity of this operation increases exponentially with the number of photons.

configuration complicates this picture, as the beam splitter simultaneously acts as mirror and as window, leaving the incident photon in a mixed state.

Tracking the output from a defined input is an exercise in combinatorics, bifurcating at each beam splitter to create an exponentially increasing set of possible outcomes. With sufficient depth the circuit creates a configurable map from input to output that is prohibitively expensive to replicate on a classical computer. When used in a hybrid approach that combines quantum computation with classical optimisation, this boson sampling scheme can be incorporated into machine learning applications, and is a leading candidate for noisy intermediate-scale quantum computing.

4 Universal quantum computing

Standard operations are abstracted in a theoretical model of quantum computing that allows algorithms to be developed independently from the physical computer. The theoretical model is implemented in the physical model via operations that represent theoretical states as physical states and interpret physical states as theoretical states, and a map that implements theoretical operations as physical operations.

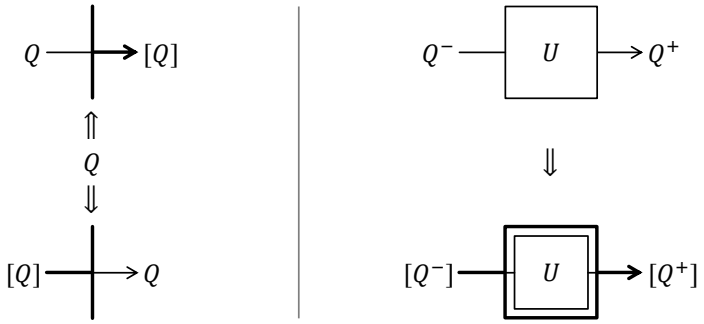


Figure 15: Implementation of the theoretical model in the physical model. The theoretical system Q is located in the physical system $[Q]$ via an operation that represents theoretical states as physical states and an operation that interprets physical states as theoretical states. The theoretical operation U is then implemented as a physical operation $[U]$. The implementation is exact when these constructions satisfy the coherence properties of natural transformations and functors.

Definition (Implementation)**.** *The implementation of the theoretical model in the physical model associates the theoretical system Q with a physical system $[Q]$ via operations that represent and interpret state:*

$$\begin{aligned} \vdash &: Q \to [Q] \\ \dashv &: [Q] \to Q \end{aligned} \tag{37}$$

satisfying the compatibility condition:

$$\vdash \circ \dashv = \iota \tag{38}$$

so that $\vdash$ is monomorphic and $\dashv$ is epimorphic. The implementation associates the theoretical operation $U : Q^- \to Q^+$ with a physical operation:

$$[U] : [Q^-] \to [Q^+] \tag{39}$$

satisfying the weak functoriality condition:

$$\vdash \circ [U_1] \circ [U_2] \circ \dashv = \vdash \circ [U_1 \circ U_2] \circ \dashv \tag{40}$$

for compatible operations. This enforces the consistency of circuit building in the theoretical and physical systems.

The theoretical operation U is implemented in the physical model as the operation $\vdash \circ [U] \circ \dashv$ constructed in three steps: represent the input theoretical state as a physical state; act on this with the physical operation; interpret the output physical state as a theoretical state. This implementation is exact *when it satisfies the weak naturality condition:*

$$\vdash \circ [U] \circ \dashv = U \tag{41}$$

Taken together, weak functoriality and weak naturality ensure that algorithms developed in the theoretical model map precisely to the physical model.

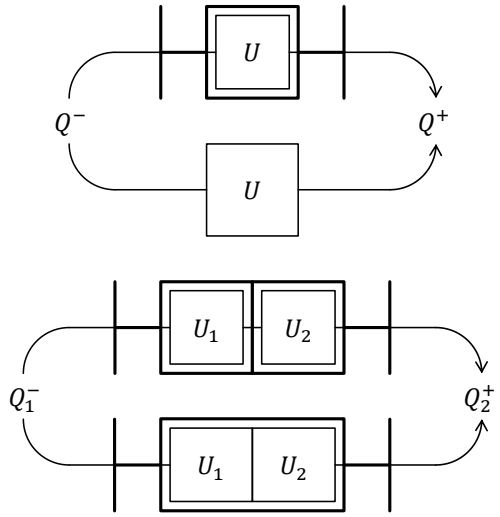


Figure 16: The weak naturality and weak functoriality properties of the implementation, expressed in these commutative diagrams, ensure that algorithms developed in the theoretical model map precisely to the physical model.

A sufficient (but not strictly necessary) condition is that the implementation is a functor:

$$[U_1 \circ U_2] = [U_1] \circ [U_2] \tag{42}$$

and that the representation $\vdash$ and interpretation $\dashv$ are compatible natural transformations:

$$\begin{aligned} U \circ \vdash &= \vdash \circ [U] \\ \dashv \circ U &= [U] \circ \dashv \end{aligned} \tag{43}$$

Naturality implies that an operation has the same effect on the state whether performed in the theoretical or physical model. Functoriality means that circuit construction in the theoretical model is mirrored in the physical model. These coherence properties are weakened by restricting to the domain of application strictly required by the implementation.

For quantum systems, the representation $\vdash$ of theoretical states as physical states is assumed to be an isometry:

$$\vdash \vdash^* = \iota \tag{44}$$

The interpretation $\dashv$ of physical states as theoretical states is then taken to be the adjoint of the isometry:

$$\dashv = \vdash^* \tag{45}$$

These maps are compatible thanks to the isometry property.

Exactness is a strong condition, and there are weaker conditions that can be imposed on the quantum implementation while still partially maintaining its utility. For the theoretical operation U with physical implementation $[U]$,



Figure 17: The properties of an implementation are expressed as commutative diagrams, in traditional form on the left and in circuit form on the right. This diagram expresses compatibility of the operations that represent and interpret states. The diagrams below describe categorical properties that are sufficient to imply exactness for the implementation.

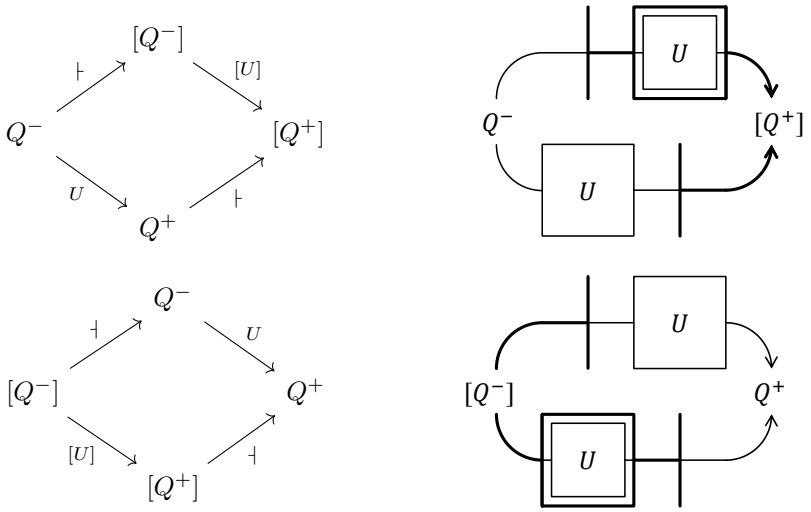


Figure 18: These commutative diagrams express naturality of the operations that represent and interpret states, ensuring that an operation has the same effect on the state in the theoretical and physical models.

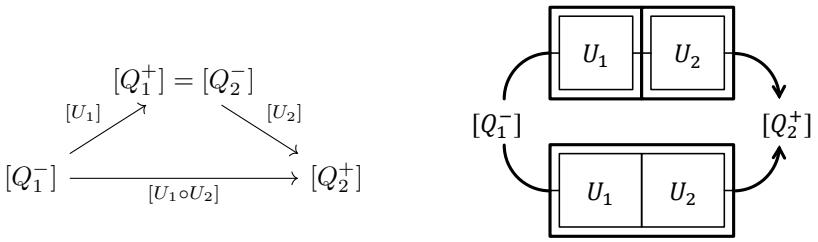


Figure 19: This commutative diagram expresses functoriality of the implementation of operations, ensuring that circuit construction in the theoretical model is mirrored in the physical model.

define the floor f and cap c to be respectively the largest and smallest scalars satisfying the inequality:

$$f\left|\langle b^-|\vdash[U]\dashv|b^+\rangle\right|^2 \leq \left|\langle b^-|U|b^+\rangle\right|^2 \leq c\left|\langle b^-|\vdash[U]\dashv|b^+\rangle\right|^2 \tag{46}$$

for all theoretical states $\langle b^-|$ and $\langle b^+|$, where $\langle b|\vdash$ denotes the physical state that represents the theoretical state $\langle b|$. The squared moduli of theoretical matrix elements are in this way bounded by computable quantities. Noting that many important quantum algorithms depend only on whether an outcome has non-zero probability, the physical operation $[U]$ is said to be *equivalent* to the theoretical operation U if these scalars satisfy:

$$0 < f \leq c < \infty \tag{47}$$

The physical computer estimates the matrix elements of $[U]$ via repeated execution; equivalence then translates this into bounds for the matrix elements of U in the theoretical computer. Performance of the computer thus depends on the accuracy of the physical estimate and the tightness of the theoretical bounds.

Calculations on the physical computer are restricted to the squared moduli of matrix elements in the computation basis of the system. It may not be possible to precisely perform the physical calculation $|\langle b^-|\vdash[U]\dashv|b^+\rangle|$, but estimatable bounds can be identified:

$$\mu - \varepsilon \leq \left|\langle b^-|\vdash[U]\dashv|b^+\rangle\right|^2 \leq \mu + \varepsilon \tag{48}$$

where:

$$\mu = \sum_{\langle n^-|}\sum_{\langle n^+|}\left|\langle b^-|\vdash n^-\rangle\right|^2\left|\langle n^-|[U]|n^+\rangle\right|^2\left|\langle n^+|\dashv b^+\rangle\right|^2 \tag{49}$$

$$\mu + \varepsilon = (\sum_{\langle n^-|}\sum_{\langle n^+|}\left|\langle b^-|\vdash n^-\rangle\right|\left|\langle n^-|[U]|n^+\rangle\right|\left|\langle n^+|\dashv b^+\rangle\right|)^2$$

summing over the preparation and measurement bases of the physical computer. Combined, the bounds on the theoretical calculation $|\langle b^-|U|b^+\rangle|$ are then:

$$f(\mu - \varepsilon) \leq \left|\langle b^-|U|b^+\rangle\right|^2 \leq c(\mu + \varepsilon) \tag{50}$$

Compatibility of the theoretical and physical computation bases thus contributes to the overall performance of the quantum computer. In particular, $\varepsilon = 0$ when each theoretical basis state maps to an unmixed physical basis state.

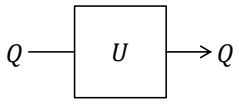
In the theoretical model of universal quantum computing the elementary system is the qudit whose state space Q is d-dimensional with computation basis:

$$\{\langle b| : b = 0, \ldots, d-1\} \tag{51}$$

where d is the arity of the model. Operations on this system are elements of the group $\mathsf{U}[d]$, the unitary maps in d dimensions. Encoding these dits in the d-ary expansion of a positive integer, the state space of the N-qudit system $\otimes^N Q$ is d^N-dimensional with computation basis:

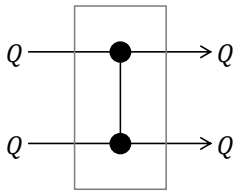
$$\{\langle b| : b = 0, \ldots, d^N - 1\} \tag{52}$$

Operations on this system are elements of the group $\mathsf{U}[d^N]$, the unitary maps in d^N dimensions. Determining whether a physical model is able to represent these operations is simplified by reducing to a smaller set of operations that generates them. Conveniently, operations of the qudit model are generated by unitary maps on a single qudit:



$$U \in \mathsf{U}[d] \tag{53}$$

and any unitary map on two qudits that does not factorise as the concatenation of two single-qudit maps. For the qubit ($d = 2$) model, a simple example is provided by the controlled-Z gate on two qubits:



$$CZ = \begin{bmatrix} 1 & 0 & 0 & 0 \\ 0 & 1 & 0 & 0 \\ 0 & 0 & 1 & 0 \\ 0 & 0 & 0 & -1 \end{bmatrix} \in \mathsf{U}[4] \tag{54}$$

Any physical model that implements this reduced set of operations implements the universal model of quantum computing.

There are many physical systems that support this theoretical model, and within a given physical system there may be multiple distinct ways to implement the model, each with its advantages and disadvantages. Specialising to photonic systems, two implementations are reviewed below: the *single-photon qubit* model, and the *parity qudit* model.

The single-photon qubit model. In this model, the state space Q of the single qubit is located within the dual-mode photonic state space $[Q] = B \otimes B$. Theoretical states are represented as photonic states via the isometry:

$$\begin{aligned} \langle 0| &= \langle 01| \\ \langle 1| &= \langle 10| \end{aligned} \tag{55}$$

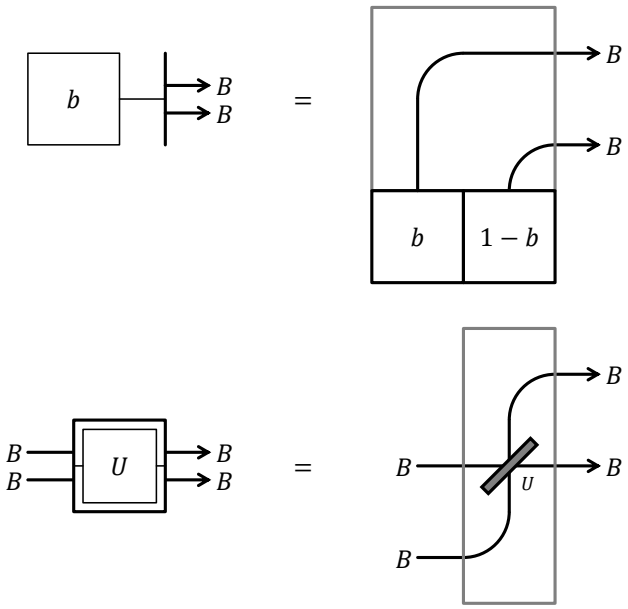
and photonic states are interpreted as theoretical states via the adjoint of this representation:

$$\begin{aligned} \langle 01| &= \langle 0| \\ \langle 10| &= \langle 1| \end{aligned} \tag{56}$$

with the other computation basis states mapping to zero. Each qubit basis state is identified with a unique computation basis state in the photonic state space. The squared modulus of the theoretical matrix element can thus be derived from the corresponding physical matrix element estimated by the photonic computer.

The single-photon qubit model is ideally suited to a machine that reliably generates and detects small numbers of photons. Physical qubits are prepared from the photon source and beam splitters are used to implement the operations of the theoretical model.

The diagrams below show how to represent qubits and implement single-qubit gates on the photonic computer. In the first diagram, the qubit is represented on two internal edges by using the input edges to introduce a single photon. In the second diagram, the single-qubit operation is performed on two internal edges without the need for interaction with the external system. Both these circuits deterministically implement the desired operation.



Problems arise in this approach when implementing non-trivial operations on multiple qubits, as the absence of photon interaction prevents these operations from being implemented directly on the internal circuit. This algorithmic shortfall is remediated by incorporating projective measurement, at the cost of losing determinism in the outcome.

The protocol originally developed by Knill, Laflamme and Milburn illustrates the key properties of quantum mechanics, and photonic systems in particular, that contribute to the creation of multi-qubit operations. The scheme is non-deterministic, requiring projective measurement, and makes use of destructive interference and states with photon number greater than one to implement the controlled-Z gate on two qubits.

There are two component operations that are combined in the scheme. The first operation, the non-linear sign gate, uses projective measurement to generate diagonal transformations on the basis states of a single mode. The second

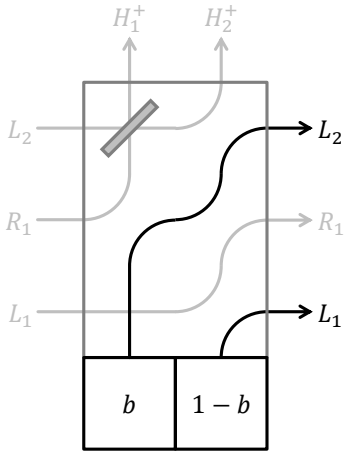


Figure 20: The abstract constructions of the single-photon qubit model can be implemented on the single-rail photonic computer. The qubit basis state $\langle b|$ is represented on two loops executed over two time-bins.

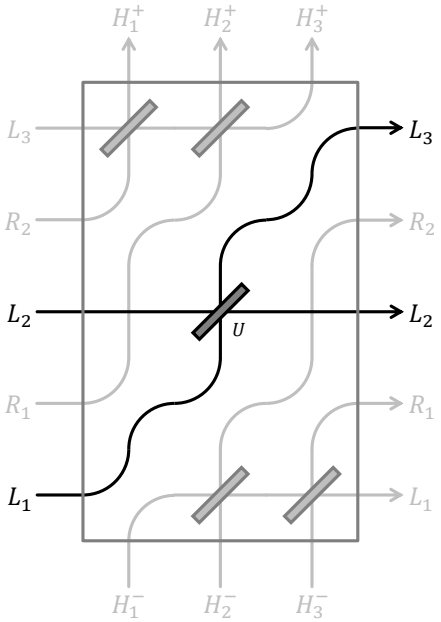
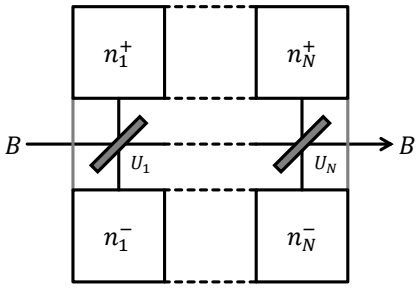


Figure 21: The theoretical operation U on a single qubit is implemented as a physical operation on the single-rail photonic computer with three loops executed over three time-bins. The input qubit is represented on the first and second loops and the output qubit is interpreted from the second and third loops. The beam splitter in the middle time-bin is configured to match the target operation.

operation, the Hadamard gate, uses destructive interference to distinguish states in two modes, effectively using states with higher photon count as holding places so that non-trivial diagonal transformations can be applied to the two-qubit state. Composing these operations allows different transformations to be applied to the four possible states of the two-qubit system.

The non-linear diagonal gate:



$$ND = \langle n_1^-|B[U_1]|n_1^+\rangle \cdots \langle n_N^-|B[U_N]|n_N^+\rangle \tag{57}$$

projects the operation of temporally-composed beam splitters, and can be implemented on the single-loop photonic computer. It is a non-deterministic gate, depending on the photon counts on the output system, though the probability of success can be optimised by using the feed-forward protocol. When the total input and output photon counts match:

$$n_1^- + \cdots + n_N^- = n_1^+ + \cdots + n_N^+ \tag{58}$$

conservation of photon number implies this gate is diagonal:

$$\langle m|ND = p[m]\,\langle m| \tag{59}$$

The phases and angles of the unitary 2-matrices associated with the beam splitters are then fine tuned to the desired action on the basis states. As a rule, each beam splitter introduces an angle that can be calibrated to a single relationship among the diagonal coefficients.

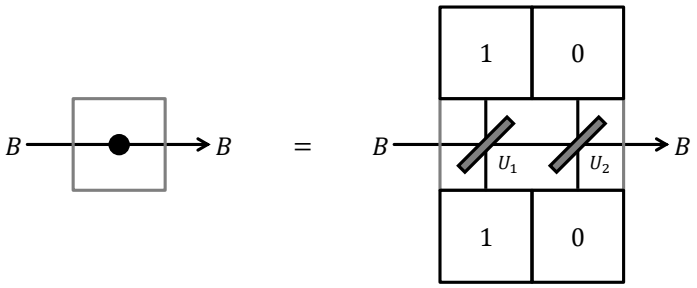
Even though the number of internal photons is unchanged by the non-linear diagonal gate, funneling the photons through a series of beam splitters forces an interaction with the external system that effects a transformation on the internal state. Aside from elementary cases, it is not possible to create these operations using linear optical components without projective measurement.

An important example is the non-linear sign gate NS, engineered using two beam splitters and one ancillary photon to impose the following relationships on states with low photon number:

$$\begin{aligned} \langle 0|NS &= p\,\langle 0| \\ \langle 1|NS &= p\,\langle 1| \\ \langle 2|NS &= -p\,\langle 2| \end{aligned} \tag{60}$$

for a positive scalar p. This operation is closed on states with at most two photons, implementing a sign change on the state with two photons. It is necessarily non-deterministic, generating the target operation on states in this subspace with probability p^2. Imposing two relationships between the coefficients,

the gate is implemented as a non-linear diagonal gate using two temporally-composed beam splitters in a circuit of the form:



$$NS = \langle 1|B[U_1]|1\rangle \langle 0|B[U_2]|0\rangle \tag{61}$$

To identify the unitary 2-matrices satisfying the target diagonal properties, first evaluate the operation for low photon number:

$$\begin{aligned}
\langle 0|NS &= e^{i(\gamma_1+\tau_1)} \cos[\theta_1] \langle 0| \\
\langle 1|NS &= -e^{i(2\gamma_1+\gamma_2-\tau_2)}(1-2\cos[\theta_1]^2)\cos[\theta_2] \langle 1| \\
\langle 2|NS &= -e^{i(3\gamma_1-\tau_1+2\gamma_2-2\tau_2)} \cos[\theta_1](2-3\cos[\theta_1]^2)\cos[\theta_2]^2 \langle 2|
\end{aligned} \tag{62}$$

then impose the phase and angle conditions:

$$\begin{aligned}
\gamma_1+\tau_1 = 2\gamma_1+\gamma_2-\tau_2 = 3\gamma_1-\tau_1+2\gamma_2-2\tau_2 = 0 \\
\cos[\theta_1] = -(1-2\cos[\theta_1]^2)\cos[\theta_2] = \cos[\theta_1](2-3\cos[\theta_1]^2)\cos[\theta_2]^2
\end{aligned} \tag{63}$$

The phase conditions are solved by:

$$\begin{aligned}
\gamma_1 &= -\tau_1 \\
\gamma_2 &= 2\tau_1+\tau_2
\end{aligned} \tag{64}$$

and the angle conditions are solved by:

$$\begin{aligned}
\cos[\theta_1] &= \sqrt{\frac{3-\sqrt{2}}{7}} \\
\cos[\theta_2] &= -\sqrt{5-3\sqrt{2}}
\end{aligned} \tag{65}$$

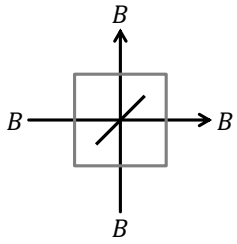
The non-linear sign gate then generates the target operation with probability:

$$p^2 = \frac{3-\sqrt{2}}{7} \tag{66}$$

This construction makes use of both the core assumptions of quantum mechanics, fine tuning the reflectance of the beam splitters to exploit the interference of photons, and applying the projective effect on the internal system of measurement on the external system.

The second operation contributing to the implementation of the controlled-Z gate is the Hadamard single-qubit gate, physically constructed by a beam

splitter configured with generating unitary matrix that maximally mixes the photon states:



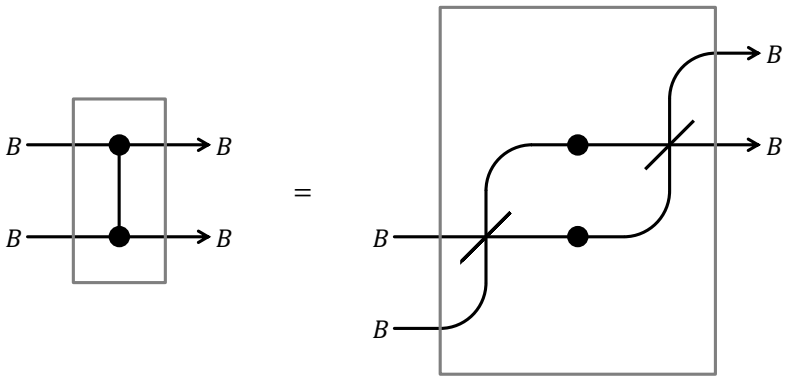
$$H = \frac{1}{\sqrt{2}} \begin{bmatrix} 1 & 1 \\ 1 & -1 \end{bmatrix} \tag{67}$$

This is an involutive operation whose action on states with low photon number is given by:

$$\begin{aligned} \langle 00|B[H] &= \langle 00| \\ \langle 01|B[H] &= \frac{1}{\sqrt{2}}(\langle 10| - \langle 01|) \\ \langle 10|B[H] &= \frac{1}{\sqrt{2}}(\langle 10| + \langle 01|) \\ \langle 11|B[H] &= \frac{1}{\sqrt{2}}(\langle 20| - \langle 02|) \end{aligned} \tag{68}$$

Destructive interference eliminates the state $\langle 11|$ in the fourth expression, a property of photonic systems first demonstrated experimentally by Hong, Ou and Mandel.

Non-linear sign gates are combined with Hadamard gates to create a non-deterministic photonic version of the controlled-Z gate:



$$CZ = B[H](NS \otimes NS)B[H] \tag{69}$$

The circuit contains two instances of the non-linear sign gate, generating the target operation with probability:

$$p^4 = \frac{11 - 6\sqrt{2}}{49} \tag{70}$$

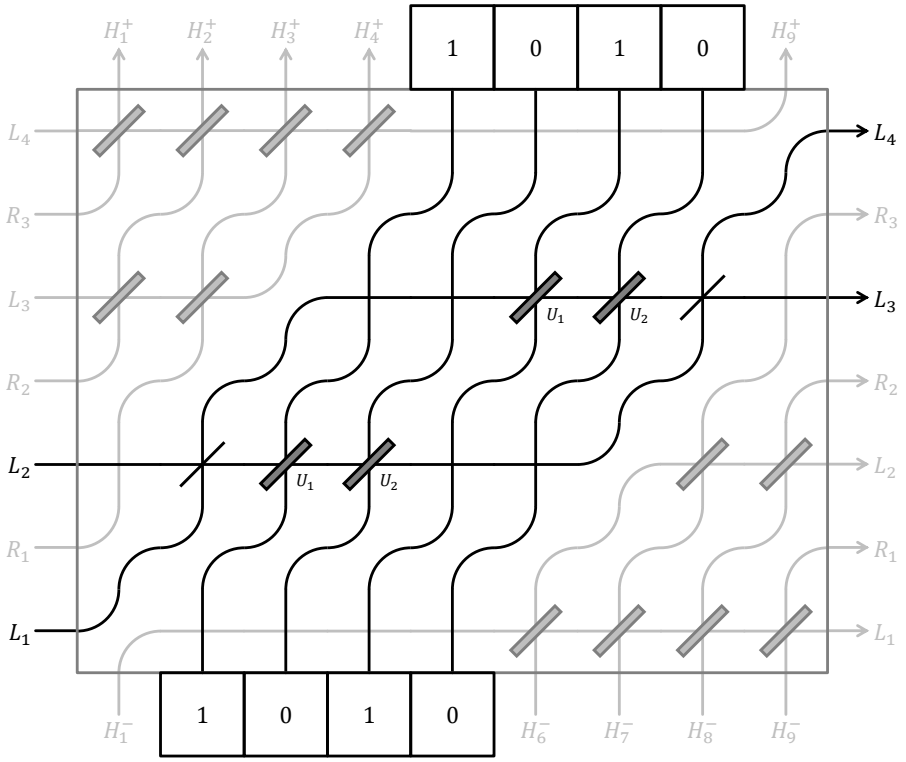
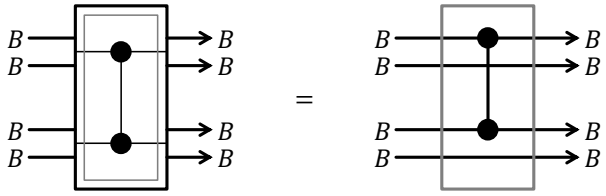


Figure 22: The photonic controlled-Z operation CZ on two qubits is implemented as a physical operation on the single-rail photonic computer with four loops executed over nine time-bins. The input qubits are represented on the first and second loops and the output qubits are interpreted from the third and fourth loops. Entanglement of the photons is created by combining Hadamard and non-linear sign gates to flip the sign when the initial internal state is $\langle 11|$. The scheme uses projective measurement, and is only successful when the output photons are counted in the specified amounts.

Tracking photons through the circuit, the photonic controlled-Z gate switches the sign of the internal basis state $\langle 11|$ but leaves the internal basis states $\langle 00|$, $\langle 01|$ and $\langle 10|$ unchanged. This gate is integrated into a circuit that exactly implements the theoretical controlled-Z gate:



There are more efficient implementations of the controlled-Z gate in the single-photon qubit model, further optimising the probability of success and constructed on simpler photonic circuits. The commonalities among these implementations are the fine tuning of the reflectances of beam splitters to exploit interference and the application of projective measurement to compensate for the lack of photon interaction. Success, which cannot be guaranteed in the scheme, is then indicated by measurements of the ancillary photons.

The parity qudit model. In this model, the state space Q of the single qudit with arity d is located within the single-mode photonic state space $[Q] = B$. Theoretical states are represented as photonic states via the isometry:

$$\langle b| = \sum_{n \bmod d = b} \alpha_n \langle n| \tag{71}$$

and photonic states are interpreted as theoretical states via the adjoint of this representation:

$$\langle n| = \alpha_n^* \langle n \bmod d| \tag{72}$$

The model is parametrised by the sequence (α_n) of scalars, normalised to ensure that the representation is isometric:

$$\sum_{n \bmod d = b} |\alpha_n|^2 = 1 \tag{73}$$

With this representation of theoretical states as physical states, the physical implementation $[U]$ of the theoretical operation U on a single qudit satisfies:

$$\mu - \varepsilon \leq \left|\langle b^-|[U]|b^+\rangle\right|^2 \leq \mu + \varepsilon \tag{74}$$

where:

$$\mu = \sum_{n^- \bmod d = b^-} \sum_{n^+ \bmod d = b^+} |\alpha_{n^-}|^2 |\alpha_{n^+}|^2 \left|\langle n^-|[U]|n^+\rangle\right|^2 \tag{75}$$

$$\mu + \varepsilon = \left(\sum_{n^- \bmod d = b^-} \sum_{n^+ \bmod d = b^+} |\alpha_{n^-}||\alpha_{n^+}| \left|\langle n^-|[U]|n^+\rangle\right|\right)^2$$

Bounds for the squared modulus of the theoretical matrix element can thus be derived from the corresponding physical matrix elements estimated by the photonic computer.

Creating physical states that represent theoretical states is challenging in this model, since they are mixtures of basis states that include all possible photon counts. Fortunately there is a version of the model that has a relatively straightforward physical implementation. This model is specified by the representation and interpretation:

$$\langle b| = \frac{1}{\sqrt{\text{exph}_b^d[|\alpha|^2]}} \sum_{n \bmod d = b} \frac{\alpha^n}{\sqrt{n!}} \langle n| \tag{76}$$
$$|n\rangle = \frac{1}{\sqrt{\text{exph}_{n \bmod d}^d[|\alpha|^2]}} \frac{\alpha^{*n}}{\sqrt{n!}} |n \bmod d\rangle$$

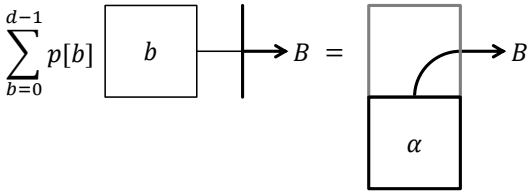
parametrised by the non-zero scalar α. The fractional exponential functions in these expressions are defined by:

$$\text{exph}_b^d[\theta] := \sum_{n \bmod d = b} \frac{\theta^n}{n!} = \frac{1}{d} \sum_{c=0}^{d-1} \exp[e^{2\pi i(c/d)}\theta - 2\pi i(bc/d)] \tag{77}$$

which reduce to the familiar hyperbolic functions in the binary case:

$$\text{exph}_0^2[\theta] = \cosh[\theta] \tag{78}$$
$$\text{exph}_1^2[\theta] = \sinh[\theta]$$

The parameter α is identified with the complex amplitude of a canonical coherent state that represents a mixed theoretical state:



$$\sum_{b=0}^{d-1} p[b] \langle b| = \langle \alpha| \tag{79}$$

The mixing weights are:

$$p[b] = \sqrt{\frac{\text{exph}_b^d[|\alpha|^2]}{\exp[|\alpha|^2]}} \tag{80}$$

and the canonical coherent state is expressed in terms of basis states as:

$$|\alpha\rangle = e^{-\frac{1}{2}|\alpha|^2} \sum_{n=0}^{\infty} \frac{\alpha^n}{\sqrt{n!}} |n\rangle$$

This is the physical state generated by an idealised laser. While it is difficult to isolate the representation of an unmixed theoretical basis state, it is possible to physically represent a mixed theoretical basis state by calibrating the laser to the specified amplitude. The limiting cases for this mixed theoretical state are:

$$\langle 0| \quad (\text{as } |\alpha| \to 0) \tag{81}$$
$$\frac{1}{\sqrt{d}} \sum_{b=0}^{d-1} \langle b| \quad (\text{as } |\alpha| \to \infty)$$

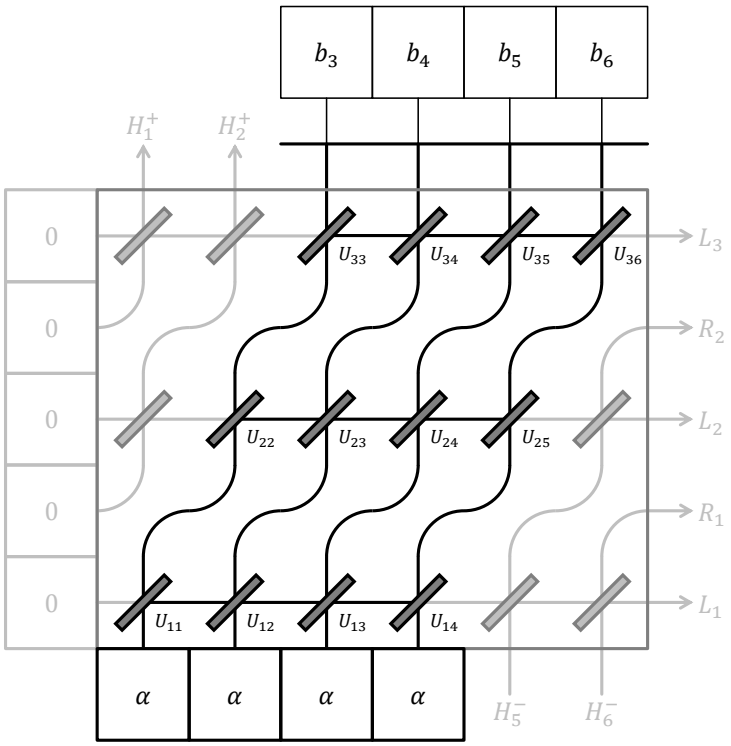


Figure 23: A boson sampling scheme based on the parity qudit model, implemented on the single-rail photonic computer with three loops executed over six time-bins. The computer is seeded using an idealised laser on the input edge and generates a ditstream on the output edge. In the application to machine learning, the reflectances of the beam splitters encode data and provide the free parameters used to train the computer.

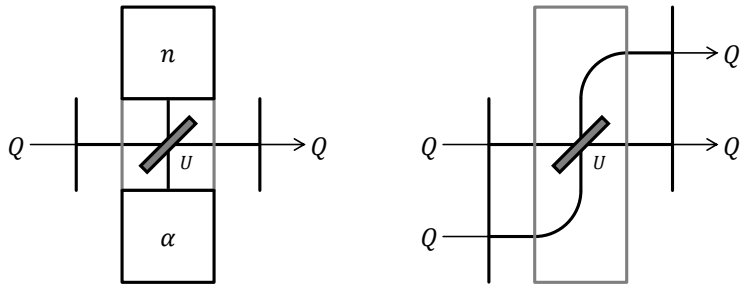
The choice of parameter α for the model thus determines the mixing of the theoretical state represented by the corresponding canonical coherent state, where the state is unmixed for small $|\alpha|$ and fully mixed for large $|\alpha|$.

Since the theoretical qudit is measured as the parity of the photon count, efficacy of the quantum computer implemented by the parity qudit model depends on the fidelity of the photon detector. A balance needs to be struck between using an amplitude large enough to generate workable mixed states while keeping the total photon count throughout the calculation low enough to ensure its parity is distinguishable by the detector.

The many-to-one interpretation of physical basis states as theoretical basis states means that theoretical matrix elements are only approximated by physical matrix elements. In spite of this drawback, the model has the advantage that any circuit can, in principle, be used as an implementation of a theoretical operation, without requiring the fine tuning that enforces only one photon on each physical qubit. Finding a family of such operations that satisfies the coherence requirements of the implementation is far from trivial, though this is

less of an issue if the operations are used in isolation, as is the case in boson sampling applications.

The beam splitter generates operations on one and two qudits:



$$\vdash \langle \alpha | B[U] | n \rangle \dashv \qquad\qquad (\vdash \otimes \vdash) B[U] (\dashv \otimes \dashv) \tag{82}$$

whose theoretical matrix elements are derived from the physical matrix elements of the beam splitter. These are valid operations on the qudit state space for any input and output photon counts on the physical circuit. Photonic circuits constructed from beam splitters access the combinatorial complexity of the full photonic state space, which grows exponentially as the circuit is expanded. This creates a rich family of operations for the parity qudit model.

5 Conclusion

The model of computing outlined in this essay uses photonic circuits to perform calculations that are computationally expensive for classical computers. The circuit is associated with the unitary N-matrix that transforms the photon creation operators on its N edges. The computer then calculates the squared moduli of the matrix elements in the n-photon representation of the unitary matrix on the N-mode bosonic Fock space, by repeatedly entering n photons on the input edges of the circuit and measuring the frequencies of the photons on the output edges.

Circuits are constructed from beam splitters by spatial composition, physically connecting two circuits at their shared edges, and temporal composition, repeatedly executing the circuit over consecutive time-bins. These compositions generate representations for unitary matrices from the unitary matrices in two dimensions. Physical limitations that challenge the implementation of this theoretical scheme include:

- The scheme depends on the ability to create photons on demand on the input edges and accurately count photons on the output edges.
- Photons on the internal edges may be lost to or gained from the external environment.
- Beam splitters are not precisely configurable, and this introduces noise into the algorithm.

Near-term applications of the photonic computer exploit the algorithmic complexity that arises from the exponential growth in the dimension of the

n-photon representation of $\mathsf{U}[N]$ as the number of photons is increased. In the boson sampling scheme, the circuit is programmed by the configurations of the beam splitters at each time-bin, and the distribution of the output photon counts is estimated by repeated execution. Including a classical optimisation loop performed outside the quantum calculation, this hybrid scheme has been proposed as an approach to quantum machine learning.

The near-term ambitions of photonic computing are curtailed by the lack of interaction between photons, preventing the full implementation of the universal quantum computer. Long-term applications resolve this shortfall by introducing additional protocols, including non-deterministic algorithms that utilise measurement of ancillary photons as operations on the internal state, and dynamic configuration of beam splitters in response to measurements of the output state. Implementation of these protocols adds theoretical and physical challenges to the development of the photonic computer.

6 Literature review

The application of category theory in quantum mechanics has a long history, with both fields developing in parallel through the twentieth century. The standard introduction to category theory is the book [25]. The modern approach to symmetric monoidal categories utilises string diagrams, with comprehensive but readable introductions in the books [7, 14]. These texts also present the ZX calculus, a theoretical cornerstone of the measurement-based approach to quantum computing. The recent paper [8] represents the ZX calculus on the bosonic state space, extending the string diagram approach to photonic computation.

Quantum computing recognises that quantum mechanics can be utilised to perform complex calculations. The history of this development is summarised in the book [27], which also introduces the high-profile algorithms that demonstrate quantum advantage and considers their implementations in real quantum systems. Developments in measurement-based quantum computing, the leading paradigm for photonic computation, are reviewed in the articles [4, 5].

Quantum information processing in photonic systems is outlined in the book [21] and the articles [22, 24, 23]. Beam splitters and phase shifters are the basic physical gates used for the construction of photonic circuits, and there is a large body of literature that discusses this; see for example [10, 6, 18, 30, 29]. The use of projective measurement to implement multi-qubit operations is introduced in the articles [19, 20], enabling the development of universal quantum computing on the photonic computer.

The focus in this essay is motivated by conversations with the team at Orca Computing, and more details on specific topics can be found in articles by the team and their collaborators. Time-bin approaches are considered in [17, 16]. The parity map is analysed in detail in the article [3], and this is used to develop novel quadratic optimisation methods as potential near-term applications of photonic computing. There is a rich and developing body of literature covering quantum machine learning and similar classical-quantum hybrid algorithms proposed as noisy intermediate-scale applications; see for example [9, 13, 1, 12, 28, 15, 26, 2, 11]. These approaches exploit quantum mechanics without necessarily requiring the full power of universal quantum computing, with a greater tolerance for the errors in near-term architectures.

References

[1] Marcello Benedetti, Erika Lloyd, Stefan Sack, and Mattia Fiorentini. Parameterized quantum circuits as machine learning models. *Quantum Science and Technology*, 4(4):043001, 2019.

[2] Kishor Bharti, Alba Cervera-Lierta, Thi Ha Kyaw, Tobias Haug, Sumner Alperin-Lea, Abhinav Anand, Matthias Degroote, Hermanni Heimonen, Jakob S Kottmann, Tim Menke, et al. Noisy intermediate-scale quantum algorithms. *Reviews of Modern Physics*, 94(1):015004, 2022.

[3] Kamil Bradler and Hugo Wallner. Certain properties and applications of shallow bosonic circuits. December 2021, 2112.09766.

[4] H. J. Briegel, D. E. Browne, W. Dür, R. Raussendorf, and M. Van den Nest. Measurement-based quantum computation. *Nature Physics 5 1, 19-26 (2009)*, October 2009, 0910.1116.

[5] Dan Browne and Hans Briegel. One-way quantum computation. *Quantum Information: From Foundations to Quantum Technology Applications*, pages 449–473, 2016.

[6] Richard A. Campos, Bahaa E. A. Saleh, and Malvin C. Teich. Quantum-mechanical lossless beam splitter: Su(2) symmetry and photon statistics. *Phys. Rev. A*, 40:1371–1384, Aug 1989.

[7] B. Coecke and A. Kissinger. *Picturing Quantum Processes*. Cambridge University Press, 2017.

[8] Giovanni de Felice and Bob Coecke. Quantum linear optics via string diagrams. April 2022, 2204.12985.

[9] Vedran Dunjko, Jacob M. Taylor, and Hans J. Briegel. Quantum-enhanced machine learning. *Phys. Rev. Lett. 117, 130501 (2016)*, October 2016, 1610.08251.

[10] H Fearn and R Loudon. Quantum theory of the lossless beam splitter. *Optics communications*, 64(6):485–490, 1987.

[11] Xun Gao, Eric R Anschuetz, Sheng-Tao Wang, J Ignacio Cirac, and Mikhail D Lukin. Enhancing generative models via quantum correlations. *Physical Review X*, 12(2):021037, 2022.

[12] Ivan Glasser, Ryan Sweke, Nicola Pancotti, Jens Eisert, and Ignacio Cirac. Expressive power of tensor-network factorizations for probabilistic modeling. *Advances in neural information processing systems*, 32, 2019.

[13] Vojtech Havlicek, Antonio D. Córcoles, Kristan Temme, Aram W. Harrow, Abhinav Kandala, Jerry M. Chow, and Jay M. Gambetta. Supervised learning with quantum enhanced feature spaces. *Nature. vol. 567, pp. 209-212 (2019)*, April 2018, 1804.11326.

[14] Chris Heunen and Jamie Vicary. *Categories for Quantum Theory: an introduction*. Oxford University Press, 2019.

[15] Hsin-Yuan Huang, Michael Broughton, Jordan Cotler, Sitan Chen, Jerry Li, Masoud Mohseni, Hartmut Neven, Ryan Babbush, Richard Kueng, John Preskill, et al. Quantum advantage in learning from experiments. *arXiv preprint arXiv:2112.00778*, 2021.

[16] Peter C. Humphreys, W. Steven Kolthammer, Joshua Nunn, Marco Barbieri, Animesh Datta, and Ian A. Walmsley. Continuous-Variable Quantum Computing in Optical Time-Frequency Modes using Quantum Memories. *Phys. Rev. Lett. 113, 130502 (2014)*, May 2014, 1405.5361.

[17] Peter C. Humphreys, Benjamin J. Metcalf, Justin B. Spring, Merritt Moore, Xian-Min Jin, Marco Barbieri, W. Steven Kolthammer, and Ian A. Walmsley. Linear Optical Quantum Computing in a Single Spatial Mode. *Phys. Rev. Lett. 111, 150501 (2013)*, May 2013, 1305.3592.

[18] M. S. Kim, W. Son, V. Bužek, and P. L. Knight. Entanglement by a beam splitter: nonclassicality as a prerequisite for entanglement. *Phys. Rev. A 65, 032323 (2002)*, June 2001, quant-ph/0106136.

[19] E. Knill, R. Laflamme, and G. Milburn. Efficient linear optics quantum computation. June 2000, quant-ph/0006088.

[20] Emanuel Knill, Raymond Laflamme, and Gerald J Milburn. A scheme for efficient quantum computation with linear optics. *nature*, 409(6816):46–52, 2001.

[21] P. Kok and B.W. Lovett. *Introduction to Optical Quantum Information Processing*. Cambridge University Press, 2010.

[22] Pieter Kok. Lecture notes on Optical Quantum Computing. *Lecture Notes in Physics 787, 187 (2009)*, May 2007, 0705.4193.

[23] Pieter Kok. Photonic Quantum Information Processing. March 2016, 1603.05036.

[24] Pieter Kok, W. J. Munro, Kae Nemoto, T. C. Ralph, Jonathan P. Dowling, and G. J. Milburn. Linear optical quantum computing with photonic qubits. *Rev. Mod. Phys.*, 79:135–174, 2007, quant-ph/0512071.

[25] S. Mac Lane. *Categories for the Working Mathematician*. Graduate Texts in Mathematics. Springer New York, 1978.

[26] Chi-Huan Nguyen, Ko-Wei Tseng, Gleb Maslennikov, H. C. J. Gan, and Dzmitry Matsukevich. Quantum-enhanced bosonic learning machine. April 2021, 2104.04168.

[27] M.A. Nielsen and I.L. Chuang. *Quantum Computation and Quantum Information: 10th Anniversary Edition*. Cambridge University Press, 2010.

[28] Jonathan Romero and Alan Aspuru-Guzik. Variational quantum generators: Generative adversarial quantum machine learning for continuous distributions. January 2019, 1901.00848.

[29] Si-Hui Tan and Peter P. Rohde. The resurgence of the linear optics quantum interferometer — recent advances and applications. May 2018, 1805.11827.

[30] Timothy Yarnall, Ayman F. Abouraddy, Bahaa E. A. Saleh, and Malvin C. Teich. Synthesis and Analysis of Entangled Photonic Qubits in Spatial-Parity Space. *Phys. Rev. Lett. 99, 250502 (2007)*, August 2007, 0708.3064.